

# Toward Long Distance, Sub-diffraction Imaging Using Coherent Camera Arrays

Jason Holloway\*, *Student Member, IEEE*, M. Salman Asif, Manoj Kumar Sharma, Nathan Matsuda, *Student Member, IEEE*, Roarke Horstmeyer, Oliver Cossairt, *Member, IEEE*, and Ashok Veeraraghavan, *Member, IEEE*

**Abstract**—In this work, we propose using camera arrays coupled with coherent illumination as an effective method of improving spatial resolution in long distance images by a factor of ten and beyond. Recent advances in ptychography have demonstrated that one can image beyond the diffraction limit of the objective lens in a microscope. We demonstrate a similar imaging system to image beyond the diffraction limit in long range imaging. We emulate a camera array with a single camera attached to an X-Y translation stage. We show that an appropriate phase retrieval based reconstruction algorithm can be used to effectively recover the lost high resolution details from the multiple low resolution acquired images. We analyze the effects of noise, required degree of image overlap, and the effect of increasing synthetic aperture size on the reconstructed image quality. We show that coherent camera arrays have the potential to greatly improve imaging performance. Our simulations show resolution gains of  $10\times$  and more are achievable. Furthermore, experimental results from our proof-of-concept systems show resolution gains of  $4\times$ – $7\times$  for real scenes. All experimental data and code is made publicly available on the project webpage. Finally, we introduce and analyze in simulation a new strategy to capture macroscopic Fourier Ptychography images in a single snapshot, albeit using a camera array.

## I. INTRODUCTION

Imaging from large stand-off distances typically results in low spatial resolution. While imaging a distant target, diffraction blur, caused by the limited angular extent of the input aperture, is the primary cause of resolution loss. As a consequence, it is desirable to use a large lens. However, telephoto lenses of comparable f-numbers ( $f/\#$ s) are typically an order of magnitude more expensive and heavier than their portrait counterparts. For example, consider imaging a subject at a distance of  $z = 1$  km with a lens aperture diameter of  $d = 12.5$  mm. Then the diffraction spot size is  $\lambda z/d \approx 50$  mm diameter diffraction blur size at the object, completely blurring out important features, such as faces. If a large lens (same focal length but with a 125 mm-wide aperture) is used instead, the diffraction blur is reduced to a 5 mm diameter, which is small enough to be enable face recognition from 1 km away. Unfortunately, such telescopic lenses are expensive and bulky, and are thus rarely used.

New computational imaging techniques are being developed to improve resolution by capturing and processing a collection

J. Holloway, M.S. Asif, and A. Veeraraghavan are with the Dept. of Electrical and Computer Engineering, Rice University, Houston, TX, 77005 USA e-mail: jh25@rice.edu

M.K. Sharma, N. Matsuda, and O. Cossairt are with the Dept. of Electrical Engineering and Computer Science, Northwestern University, Evanston, IL, 60208.

R. Horstmeyer is with the Dept. of Electrical Engineering, California Institute of Technology, Pasadena, CA, 91125.

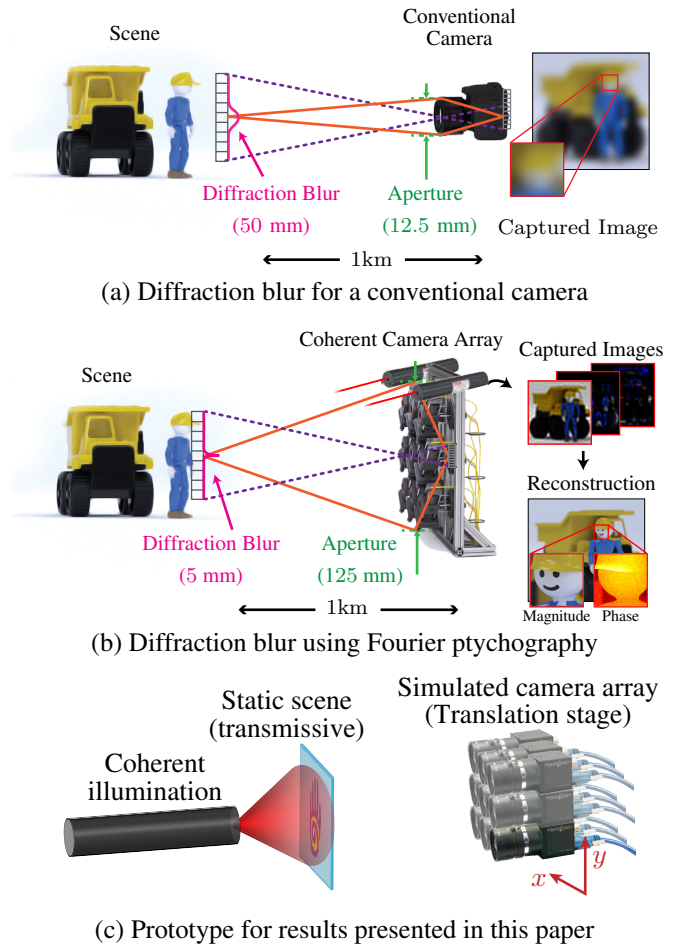


**Fig. 1. Using active illumination to overcome the diffraction limit in long range imaging.** Diffraction blur is the primary cause of resolution loss in long distance imaging. Consider this illustration of imaging a human-sized object 1 km away. (a) A conventional camera using passive illumination with a fixed aperture size of 12.5 mm induces a diffraction spot size of 50 mm on objects 1 km away, destroying relevant image features. (b) Using Fourier ptychography, an array of cameras using coherent illumination creates a synthetic aperture 10 times larger than (a) resulting in a diffraction spot size of 5 mm for scenes 1 km away. Phase retrieval algorithms recover the high resolution image. (c) In this paper, we present experimental results captured using a table-top prototype which can be used to simulate many of the properties of the desired system in (b).

of images. Here, we focus on one such multi-image fusion technique designed specifically for the problem of recovering image details well below the diffraction limit. It is convenient to perform multi-image fusion with a camera array, which can simultaneously acquire multiple images from different perspectives. While camera arrays such as PiCam [63] and

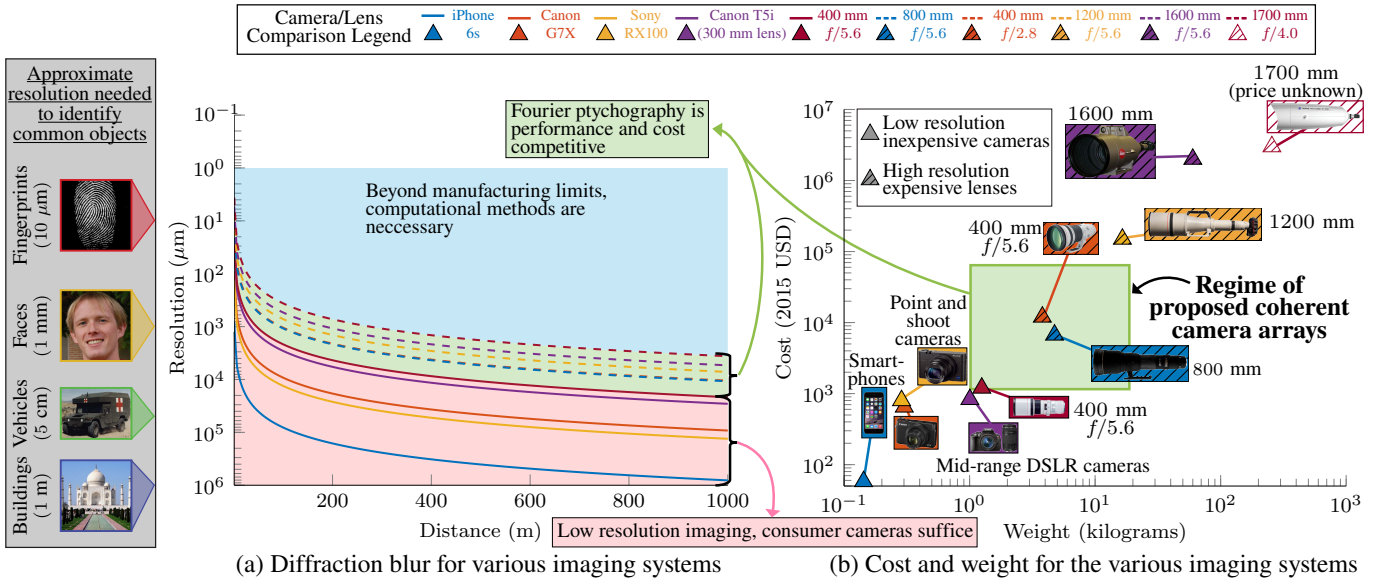


Fig. 2. **Diffraction blur limits in long distance imaging.** (a) Diffraction blur spot size as a function of distance for common and exotic imaging systems. Consumer cameras (shaded in the pink region) are designed for close to medium range imaging but cannot resolve small features over great distances. Professional lenses (green region) offer improved resolution but are bulky and expensive. Identifying faces 1 kilometer away is possible only with the most advanced super telephoto lenses, which are extremely rare and cost upwards of \$2 million US dollars [64]. Obtaining even finer resolution (blue region) is beyond the capabilities of modern manufacturing; the only hope for obtaining such resolution is to use computational techniques such as Fourier ptychography. (b) Affordable camera systems (solid marks) are lightweight but cannot resolve fine details over great distances as well as professional lenses (striped marks) which are heavy and expensive. We propose using a camera array with affordable lenses and active lighting to achieve and surpass the capabilities of professional lenses. Note: These plots only account for diffraction blur and do not consider other factors limiting resolution (see TABLE I for more details).

Light<sup>1</sup> are becoming increasingly popular and have demonstrated resolution improvement, their applications are typically limited to improving resolution limits imposed by pixel sub-sampling. They do not naturally extend to overcome the limits of diffraction blur.

Recent advances in ptychography have demonstrated that one can image beyond the diffraction limit of the objective lens in a microscope [67]. Ptychography typically captures multiple images using a programmable coherent illumination source, and combines these images using an appropriate phase retrieval algorithm. It is also possible to implement ptychography by keeping the illumination source fixed, and instead spatially shifting the camera aperture [10]. Under this interpretation, ptychography closely resembles the technique advocated in this paper to improve resolution via a “coherent camera array”. The goal of such a coherent array would be to recover both the amplitude and the phase of an optical field incident upon multiple spatially offset cameras, across the entire angular extent of the array. This matches the goal of creating a synthetic aperture via holography [26], [42], [43], but without directly measuring the phase of the incident field.

In this paper, we explore the utility of ptychography-based methods for improving the imaging resolution in long-range imaging scenarios [10]. We analyze reconstruction performance under various scenarios to study the effects of noise, required degree of image overlap, and other important parameters and show that under practical imaging scenarios, coherent camera arrays have the potential to greatly improve imaging performance. Further, we build a table-top prototype (shown in Fig. 1c) and show real results of several subjects,

demonstrating up to a  $7\times$  quantitative improvement in spatial resolution. While confined to imaging within a lab, the prototype can be used to simulate many of the properties that we advocate for in a coherent camera array. Finally, we demonstrate that multiplexed illumination can be used to build a coherent camera array capable of capturing scenes in a single snapshot.

## II. RESOLUTION LIMITATIONS IN LONG RANGE IMAGING

Image resolution at long ranges is limited due to several inter-related factors as seen in TABLE I. We classify these factors as being intrinsic to the imaging system (e.g. diffraction) and extrinsic to the imaging system (e.g. turbulence).

**Pixel Size:** A number of prior works developed techniques to overcome pixel-limited resolutions by capturing a sequence of images with sub-pixel translations [4]. Some translation between the camera and scene is required between each exposure. This is achieved using either small sensor movements, lens defocus, or movements of the entire imaging system [2]. A sequence of sub-pixel shifted images may be acquired in a single snapshot by using a camera array. However, current sensor pixels are approaching the diffraction limit of visible light (1.2  $\mu\text{m}$  pixels are commercially widespread), and thus pixel sampling limits are not as critical a limitation to many current and future imaging platforms as in the past.

**Diffraction:** Perhaps the most challenging impediment to imaging high resolution at a large distance is optical diffraction caused by the finite aperture size of the primary imaging lens. While a wider lens will lead to a sharper point-spread function for a fixed focal length, it will also create proportionally larger aberrations. Additional optical elements may be added to the lens to correct these aberrations, but these elements

<sup>1</sup><http://light.co>

TABLE I  
INTRINSIC AND EXTRINSIC FACTORS WHICH LIMIT RESOLUTION IN LONG RANGE IMAGING

Resolution Limit	Primary Cause	Intrinsic/Extrinsic	Example solutions
<b>Diffraction (this paper)</b>	<b>Finite aperture acceptance angle</b>	<b>Intrinsic</b>	<b>Synthetic aperture via holography, ptychography</b>
Sampling	Finite pixel size	Intrinsic	Multi-image super-resolution [47], dithering [19], camera arrays [65]
Aberrations	Finite lens track length/ design complexity	Intrinsic	Additional optical elements, precalibration and digital removal [56], [32], adaptive optics [3]
Noise	Sensor readout, shot noise	Intrinsic/Extrinsic	Image averaging, denoising [8]
Turbulence	Air temperature, wind shear	Extrinsic	Adaptive optics [13], lucky imaging [18], [31], [54]
Motion	Camera and/or scene motion	Extrinsic	Flutter shutter [28], [53], invariant blur [35]

will increase the size, weight and complexity of the imaging system [38]. As noted in the introduction, the main focus of this work is to address this diffraction-based resolution limit with a joint optical capture and post-processing strategy. We use a small, simple lens system to capture multiple intensity images from different positions. In our initial experiments our prototype uses a single camera on a translation stage that captures images sequentially (in approximately 90 minutes). The next phase of our research will focus on design, assembly, and calibration of a snapshot-capable camera array system. We fuse captured images together using a ptychographic phase retrieval algorithm. The result is a high resolution complex reconstruction that appears to have passed through a lens whose aperture size is equal to the synthetic aperture created by the array of translated camera positions.

**Additional causes of resolution loss:** We do not explicitly address the four remaining causes of resolution loss in this work. We now mention their impact both for completeness and to highlight additional alternative benefits of the ptychographic technique. First, intrinsic lens aberrations limit the resolution of every camera. Second, turbulence is a large source of image degradation, especially when long exposure times are required. Finally, noise and possible motion during the camera integration time leads to additional resolution loss.

While not examined here, ptychography captures redundant image data that may be used to simultaneously estimate and remove microscope [49] or camera [30] aberrations. Redundant data is also helpful to address noise limits. Furthermore, while yet to be demonstrated (to the best of our knowledge), is not hard to imagine that similar computational techniques may help estimate and remove external aberrations caused by turbulence, especially as our procedure simultaneously recovers the incident field’s phase. Ptychographic techniques thus appear ideally suited for overcoming the long-distance image resolution challenges summarized in TABLE I. In this paper, we address a limited problem statement; namely, can a ptychographic framework be extended to achieve sub-diffraction resolution at large standoff distances?

### III. RELATED WORK

Computationally improving camera resolution is a long-standing goal in imaging sciences. Here, we summarize the prior work most relevant to our coherent camera array setup.

**Multi-Image Super-Resolution:** Multi-image super-resolution has received much attention over the past 20 years (see [47] for a comprehensive survey of the field)

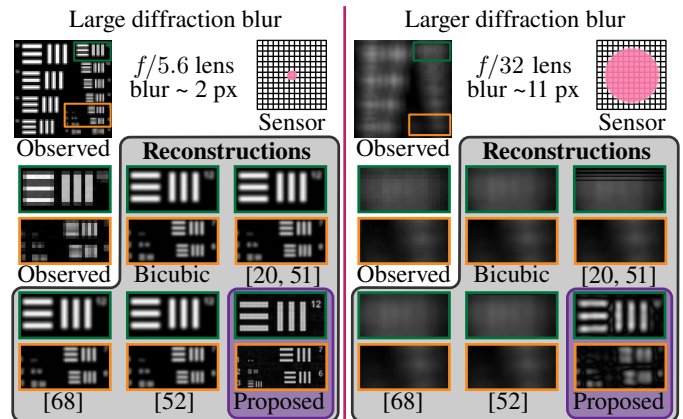


Fig. 3. **Comparison with multi-image super-resolution under large diffraction blur** Left: When diffraction blur is not much larger than a pixel, conventional multi-image super-resolution methods achieve a  $2\times$  improvement in resolution while the proposed method offers a  $4\times$  improvement in this example (greater resolution improvements are shown in Section VI and Section VII). Right: Under extreme diffraction blur, conventional methods break down and offer no improvement. Only with the proposed method can distinct image features be recovered. The diffraction spot size for each scenario is represented by the pink circle on the sensor grid; the high resolution ground truth image is presented in Fig. 4.

and continues to be an important area of study in modern camera arrays [7], [63]. However, the overall improvement in resolution has been modest; practical implementations achieve no more than a  $2\times$  improvement [1], [37], [46]. Exemplar based efforts to improve the super-resolution factor beyond 2 use large dictionaries to hallucinate information [17], [22] and offer no guarantees on fidelity. Even these techniques are typically limited to producing a  $4\times$  improvement in resolution [22]. In this paper, we present a technique that can, in theory, improve resolution all the way to the diffraction limit of light (e.g. below a micron for visible light). Our experimental results clearly indicate significant resolution enhancements over and above those achieved by traditional multi-image techniques, particularly in the regime of large diffraction blur.

In Fig. 3, we simulate super-resolution gains using a conventional imaging system and our proposed imaging system. A  $512 \times 512$  pixel resolution target (shown in full in Fig. 4) is imaged onto a  $64 \times 64$  pixel sensor with a pixel pitch of  $2 \mu\text{m}$ , for an  $8\times$  loss in resolution. In the left column of Fig. 3, a lens with a large aperture ( $f/5.6$ ) produces a diffraction spot size of  $3.7 \mu\text{m}$ . Due to the pixel sampling, the smallest discernible features belong to group 12. Common

multi-image super-resolution techniques such as Papoulis-Gerchberg super-resolution [20], [51], robust super-resolution [68], and normalized convolution [52] yield comparable  $2\times$  improvement, resolving features in group 6. These algorithms are implemented using code made available from [62]. Active super-resolution provides even greater resolution, resolving features down to group 3, for a four-fold improvement (purple box). Full details regarding the proposed image acquisition and recovery process will be provided in subsequent sections.

In the presence of large diffraction blur, conventional super-resolution methods fail to improve spatial resolution to any appreciable degree. Fig. 3 (right) illustrates the same imaging scenario as before, but using a lens with smaller diameter. Using a  $f/32$  lens results in diffraction blur of  $21.5\ \mu\text{m}$ . Conventional methods fail to recover any spatial information, whereas our proposed active imaging system can resolve features in group 12 and separates the smaller groups into distinct features. In this paper we will restrict our scope to the regime of large diffraction blur, where conventional super-resolution methods are ill-suited for improving resolution; however, the proposed solution may also improve spatial resolution for imaging systems with small diffraction blur.

**Camera Arrays:** Camera arrays comprised of numerous ( $>10$ ) cameras, have been proposed as an efficient method of achieving a depth-of-field that is much narrower than that of a single camera in the array. Large arrays, such as the Stanford camera array [65], demonstrated the ability to computationally refocus. Camera arrays are also well-suited to astronomical imaging. The CHARA array [58] is an collection of telescopes (1 meter diameter) on Mount Wilson in California which are jointly calibrated to resolve small astronomical features (angular resolution of 200 microarcseconds), using a synthetic aperture with a diameter of 330 meters.

Despite the advantages provided using a camera array, diffraction blur limits resolution in long distance imaging. For scenes lit with incoherent illumination, such as sunlight, multi-image super-resolution techniques can further increase spatial resolution by a factor of two. Even with this modest improvement in resolution, the remaining blur due to diffraction may still preclude recovering fine details. In this paper we propose using active illumination to recover an image with spatial resolution many times greater than the limit imposed by optical diffraction.

**Fourier Ptychography** Fourier ptychography (FP) has permitted numerous advances in microscopy, including wide-field high-resolution imaging [67], removing optical [30] and pupil [49] aberrations, digital refocusing [10], and most recently 3D imaging of thick samples [36], [61]. While most FP microscopy methods are transmissive, there is a nascent interest in reflective mode ptychography [57], [24], though we know of no FP work for far field imaging. FP is, in effect, a synthetic aperture technique [26], [42], [43], [45] that does not require phase measurements. In FP microscopy, the imaging lens is often fixed while an array of light sources is used to shift different regions of the image spectrum across a fixed aperture of limited size. Instead of advancing the light in a raster pattern, the illumination sources may be multiplexed to increase SNR and reduce acquisition time [11],

[60]. Refinements in the sampling pattern can also reduce acquisition time [23]. Initial work in macroscopic imaging [10] suggests the potential benefits of Fourier ptychography in improving spatial resolution of stand-off scenery. In this paper we extend upon this work and characterize how the amount of overlap, synthetic aperture size, and image noise affects reconstruction quality and resolution improvement. Furthermore, we describe early efforts towards realizing a physical system to beat diffraction in long range snapshot imaging systems.

**Phase Retrieval Algorithms:** Phase retrieval is a required component of ptychographic image reconstruction. Image sensors record the magnitude of a complex field, either in the Fourier domain for traditional ptychography or the spatial domain in Fourier ptychography. Numerous algorithms for retrieving the missing phase information have been proposed. One of the simplest techniques is based upon alternating projections [21], [16]. Many extensions of this simple starting point exist for both standard phase retrieval using a single image [14], [15], as well as ptychographic phase retrieval using multiple images [29], [40].

**Alternative methods to improve resolution:** The primary technique to improve image resolution in long-distance imaging is to simply build a larger telescope. On the scale of portable imaging systems, this typically means removing large glass optical elements in favor of catadioptric lens designs, where a mirror reflects light through a much smaller lens. Other techniques for improving resolution include lucky imaging to mitigate atmospheric turbulence [18], [31], [66] in terrestrial imaging. In astronomical imaging, motion tracking [9], [44] and speckle imaging [34], [33], [39] are common methods to improve image resolution. These latter approaches tackle external factors limiting resolution, but do not address the effects of diffraction on spatial resolution.

#### IV. FOURIER PTYCHOGRAPHY FOR LONG RANGE IMAGING

Our goal in this paper is to capture high resolution images of objects that are a considerable distance away from the camera, e.g. resolve a face 1000 meters away. Passive camera systems use available (incoherent) illumination sources such as the sun and suffer from significant diffraction blur. Existing super resolution methods may be able to effectively reduce the amount of blur by a factor of two, which may be insufficient to resolve enough detail to recover the object of interest. In order to resolve even smaller features, we assume that we have a coherent or partially coherent illumination source; that is, we have active illumination.

Like other multi-image super-resolution methods [1], [37] we will capture a series of low resolution images which we will then use to recover a high resolution image. We take multiple images using a coherent illumination source where each image is from a different (known) position in the  $XY$  plane. For simplicity we assume the camera positions coincide with a regular grid, though this is not necessary [23]. It should be noted that we would obtain the same result by leaving the camera stationary and moving the illumination source, a common practice in microscopy [11], [29], [49], [60], [61].

### A. Image Formation Model

We first assume a single fixed illumination source<sup>2</sup>, which can either be co-located with or external to our imaging system. The source should be quasi-monochromatic, with center wavelength  $\lambda$ . For color imaging, multiple quasi-monochromatic sources (i.e., laser diodes) are effective [67]. The source emits a field that is spatially coherent across the plane which contains our object of interest,  $P(x, y)$ . We assume this plane occupies some or all of the imaging system field of view.

The illumination field,  $u(x, y)$ , will interact with the object, and a portion of this field will reflect off the object towards our imaging system. For our initial experiment, we assume the object is thin and may be described by the 2D complex reflectivity function  $o(x, y)$ . While we discuss 2D surfaces, extension to surface reflectance from 3D objects follows from this analysis, see [57], [61], [36] for examples of 3D FP microscopy. Under the thin object approximation, the field emerging from the object is given by the product  $\psi(x, y) = u(x, y)o(x, y)$ . This then propagates a large distance  $z$  to the far field, where our imaging system occupies the plane  $S(x', y')$ .

Under the Fraunhofer approximation, the field at  $S(x', y')$  is connected to the field at the object plane by a Fourier transform [5]:

$$\hat{\psi}(x', y') = \frac{e^{jkz} e^{\frac{jk}{2z}(x'^2 + y'^2)}}{j\lambda z} \mathcal{F}_{1/\lambda z} [\psi(x, y)] \quad (1)$$

where  $k = 2\pi/\lambda$  is the wavenumber and  $\mathcal{F}_{1/\lambda z}$  denotes a two dimensional Fourier transform scaled by  $1/\lambda z$ . For the remainder of this manuscript, we will drop multiplicative phase factors and coordinate scaling from our simple model. We note that the following analysis also applies under the Fresnel approximation (i.e., in the near field of the object), as supported by recent investigations in X-ray ptychography [12], [59].

The far field pattern, which is effectively the Fourier transform of the object field, is intercepted by the aperture of our camera. We describe our limited camera aperture using the function  $A(x' - c_{x'}, y' - c_{y'})$ , which is centered at coordinate  $(c_{x'}, c_{y'})$  in the plane  $S(x', y')$  and passes light with unity transmittance within a finite diameter  $d$  and completely blocks light outside (i.e., is a ‘‘circ’’ function).

The optical field immediately after the aperture is given by the product  $\hat{\psi}(x', y')A(x' - c_{x'}, y' - c_{y'})$ . This bandlimited field then propagates to the image sensor plane. Again neglecting constant multiplicative and scaling factors, we may also represent this final propagation using a Fourier transform. Since the camera sensor only detects optical intensity, the image measured by the camera is

$$I(x, y, c_{x'}, c_{y'}) \propto \left| \mathcal{F} \left[ \hat{\psi}(x', y')A(x' - c_{x'}, y' - c_{y'}) \right] \right|^2. \quad (2)$$

In a single image, the lowpass nature of the aperture results in a reduced resolution image. For an aperture of diameter  $d$  and focal length  $f$ , diffraction limits the smallest resolvable feature within one image to be approximately  $1.22\lambda f/d$ .

<sup>2</sup>In Section VIII we consider multiple illumination sources

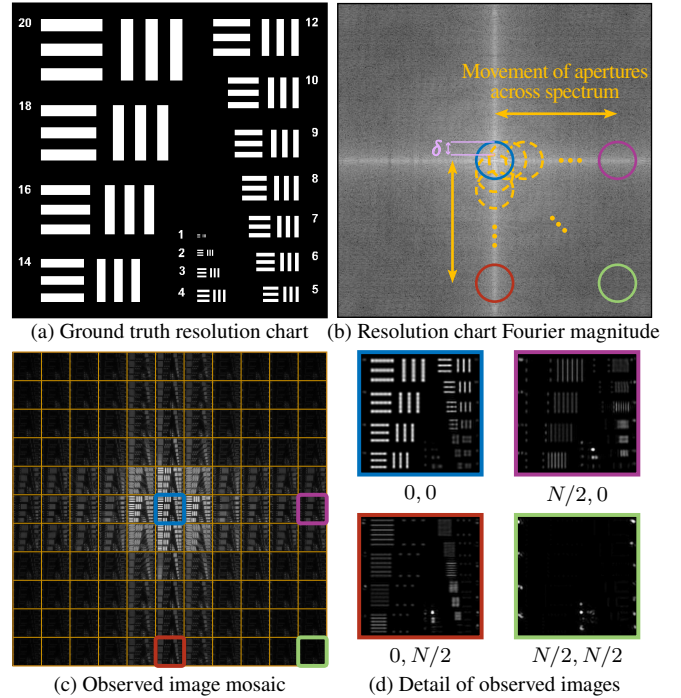


Fig. 4. **Sampling the Fourier domain at the aperture plane.** For a given high resolution target (a), the corresponding Fourier transform is formed at the aperture plane of the camera (b). The lens aperture acts as a bandpass filter, only allowing a subset of the Fourier information to pass to the sensor. A larger aperture may be synthesized by scanning the aperture over the Fourier domain and recording multiple images. (c) The full sampling mosaic acquired by scanning the aperture. The dynamic range has been compressed by scaling the image intensities on a log scale. (d) Larger detail images shown of four camera positions, including the center. Image intensities have been scaled linearly, note that only high frequency edge information is present in the three extreme aperture locations. Please view digitally to see details.

### B. Fourier Ptychography to Improve Resolution

Ptychography presents one strategy to overcome the diffraction limit by capturing multiple images and synthetically increasing the effective aperture size. The series of captured images is used to recover the high resolution complex field in the aperture plane and subsequently a high resolution image.

To achieve this, we re-center the camera at multiple locations,  $(c_{x'_i}, c_{y'_i})$ , and capture one image at the  $i$ th camera location, for  $i = 1, \dots, N$ . This transforms (2) into a four-dimensional discrete data matrix. The  $N$  images can be captured in a number of ways, one can: physically translate the camera to  $N$  positions, construct a camera array with  $N$  cameras to simultaneously capture images, fix the camera position and use a translating light source, or use arbitrary combinations of any of these techniques.

If we select our aperture centers such that they are separated by the diameter  $d$  across a rectilinear grid, then we have approximately measured values from the object spectrum across an aperture that is  $\sqrt{N}$  times larger than what is obtained by a single image. Thus, it appears that such a strategy, capturing  $N$  images of a coherently illuminated object in the far field, may be combined together to improve the diffraction-limited image resolution<sup>3</sup> to  $1.22\lambda f/\sqrt{N}d$ .

<sup>3</sup>It should be noted that it is not possible to improve resolution below the diffraction limit of the light source  $1.22\lambda/2$ , though practical considerations will prevent this from being a concern in macroscopic FP

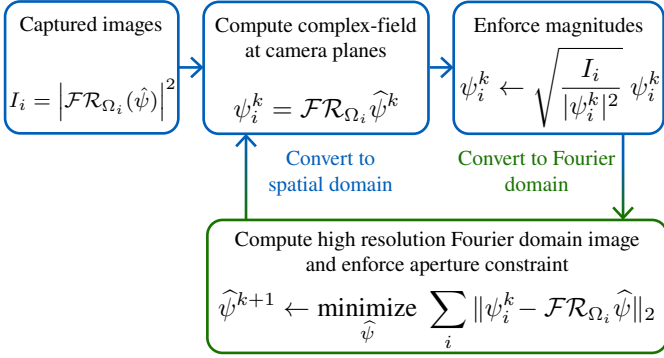


Fig. 5. **Block diagram of the image recovery algorithm.** Constraints on the image domain magnitude and Fourier domain support are enforced in an alternating manner until convergence or a maximum iteration limit is met.

However, since our detector cannot measure phase, this sampling strategy is not effective as-is. Instead, it is necessary to ensure the aperture centers overlap by a certain amount (i.e., adjacent image captures are separated by a distance  $\delta < d$  along both  $x'$  and  $y'$ ). This yields a certain degree of redundancy within the captured data, which a ptychographic post-processing algorithm may utilize to simultaneously determine the phase of the field at plane  $S(x', y')$ . Typically, we select  $\delta \sim 0.25d$ . See Fig. 4 for an overview of the sampling strategy and example images recorded with the aperture acting as a bandpass filter of the Fourier transform  $\psi(x', y')$ . Next, we detail a suitable post-processing strategy that converts the data matrix  $I(x, y, c_{x'_i}, c_{y'_i})$  into a high-resolution complex object reconstruction.

## V. ALGORITHM FOR IMAGE RECOVERY

Using our coherent camera array measurements in (2), our goal is to recover the complex-valued, high-resolution field  $\psi(x', y')$ . Let us denote the image measured with camera at location  $(c_{x'_i}, c_{y'_i})$  as

$$I_i = |\psi_i|^2 \equiv |\mathcal{FR}_{\Omega_i}\hat{\psi}|^2, \quad (3)$$

where  $\psi_i = \mathcal{FR}_{\Omega_i}\hat{\psi}$  denotes the complex-valued, bandlimited field whose intensity is measured at the image sensor,  $\hat{\psi}$  denotes the complex-valued field at the Fourier plane (i.e. the aperture plane), and  $\mathcal{R}_{\Omega_i}\hat{\psi}$  denotes an aperture operator that sets all the entries of  $\hat{\psi}(x', y')$  outside the set  $\Omega_i = \{(x, y) : |x - c_{x'_i}|^2 + |y - c_{y'_i}|^2 \leq d/2\}$  to zero.

To recover the high-resolution  $\hat{\psi}$  from a sequence of  $N$  low-resolution, intensity measurements,  $\{I_i\}_{i=1}^N$ , we use an alternating minimization-based phase retrieval problem that is depicted in Fig. 5. The recovery algorithm is based on the error-reduction phase retrieval algorithm proposed by Gerchberg and Saxton [21], which continues to form the basis of many modern FP algorithms [61]. We seek to solve the following problem

$$\hat{\psi}^* = \arg \min_{\hat{\psi}} \sum_i \left\| \psi_i - \mathcal{FR}_{\Omega_i}\hat{\psi} \right\|_2 \quad \text{s.t.} \quad |\psi_i|^2 = I_i, \quad (4)$$

by alternatively constraining the support of  $\hat{\psi}$  and the squared magnitudes of  $\psi$ . We set the initial estimate of  $\hat{\psi}^0$  to be a scaled version of the Fourier transform of the mean of the

low resolution images. At every iteration ( $k$ ), we perform the following three steps:

1. Compute complex-valued images at the sensor plane using the existing estimate of the field at the Fourier plane,  $\hat{\psi}^k$ :

$$\psi_i^k = \mathcal{FR}_{\Omega_i}\hat{\psi}^k \quad \text{for all } i.$$

2. Replace the magnitudes of  $\psi_i^k$  with the magnitude of the corresponding observed images  $I_i$ :

$$\psi_i^k \leftarrow \sqrt{\frac{I_i}{|\psi_i^k|^2}} \psi_i^k \quad \text{for all } i.$$

3. Update the estimate of  $\hat{\psi}$  by solving the following regularized, least-squares problem:

$$\hat{\psi}^{k+1} \leftarrow \underset{\hat{\psi}}{\text{minimize}} \sum_i \left\| \psi_i^k - \mathcal{FR}_{\Omega_i}\hat{\psi} \right\|_2^2 + \tau \|\hat{\psi}\|_2^2, \quad (5)$$

where  $\tau > 0$  is an appropriately chosen regularization parameter. Tikhonov regularization is used for numerical stability during reconstruction as in [61]. This problem has a closed form solution, which can be efficiently computed using fast Fourier transforms.

## VI. PERFORMANCE ANALYSIS AND CHARACTERIZATION

Accurate retrieval of optical phase requires redundant measurements. If the final high-resolution image is comprised of  $n$  pixels that contain both intensity and phase information, then it is clear that we must acquire at least  $2n$  measurements of optical intensity from the image sensor. However, it is not clear if additional data should be acquired (for example to improve tolerance to noise), how much this additional data might improve the quality of our reconstructions at different resolution scales, or how many images on average might be required to achieve a certain resolution goal. We now explore these questions via simulation.

### A. Fundamental Factors that Affect Recovery Performance

There are two parameters that will influence the number of required images. The first consideration is the desired resolution limit of our coherent camera array (i.e., its minimum resolvable feature), which is equivalent to specifying the synthetic aperture size. The second consideration is the desired degree of data redundancy, which is equivalent to specifying the amount of overlap between adjacent images when viewed in the Fourier domain. Computational cost is proportional to the number of acquired images, so the user will be eventually forced to trade off reconstruction quality for reconstruction time.

### B. Experimental Design

To explore these two parameters, we perform experimental simulations using a 512 px  $\times$  512 px resolution chart shown in Fig. 4(a). This chart contains line pairs with varying widths from 20 pixels down to 1 pixel, corresponding to line pairs per pixel in the range  $[0.025, 0.5]$ . We assume each object is under coherent plane wave illumination from a distant source. Diffraction blur is determined solely by the wavelength of the coherent source and the ratio between the focal length and

aperture diameter (i.e. the  $f/\#$ ). Recall that the radius of the diffraction spot size on the sensor is approximately  $1.22\frac{\lambda f}{d}$ . We assume that the illumination wavelength is 550 nm, the focal length of the lens is 800 mm, and the aperture diameter is 18 mm. The resolution chart itself is 64 mm  $\times$  64 mm and is located 50 meters away from the camera. The aperture of the imaging system is scanned across the Fourier plane to generate each bandpassed optical field at the image plane. A pictorial representation of the sampling pattern and resulting captured images is shown in Fig. 4(b)-(d).

For simplicity, we treat the target resolution chart as an amplitude object, which may be considered to be printed on a thin glass substrate or etched out of a thin opaque material. We use the iterative algorithm described in Section V to recover the complex field of the resolution chart. The algorithm terminates whenever the relative difference between iterations falls below  $10^{-5}$  or after 1000 iterations. To quantify the reconstruction we compute the contrast for the horizontal and vertical bars belonging to each group. Contrast,  $C$ , is defined as

$$C = \frac{\bar{w} - \bar{b}}{\bar{w} + \bar{b}}, \quad (6)$$

where  $\bar{w}$  and  $\bar{b}$  denote the average intensity of the white and black bars respectively. To aid our discussion, we define the limit of resolvability to be when the contrast of a group drops below 20% (MTF20). For the simulation experiments, we will assume the image sensor has a pixel width of 2  $\mu$ m. It is important to note that in the simulation experiments we will only consider the effects of diffraction blur as the factor which limits resolution in long range images.

In our first simulation experiment, we capture a  $21 \times 21$  grid of images with 61% overlap between neighboring images. Each captured image is 512 px  $\times$  512 px, but high frequency information has been lost due to the bandpass filter. Under this setup the Synthetic Aperture Ratio (SAR), given as the ratio between the synthetic aperture diameter and lens aperture diameter, is 8.8. Fig. 6(b) shows the center observed image of the resolution target, in which features smaller than 12 pixels are lost, due to the low-pass filtering of the aperture. This corresponds to the best resolution that can be achieved in coherent illumination without using ptychography to recover additional frequency information. If we use ptychography and phase retrieval, the resolution increases significantly; features as small as 2 pixels can be recovered as shown in Fig. 6(d). Plots comparing the contrast of the image intensity for the center observation (dashed blue line) and the recovered image (solid purple line) are provided in Fig. 6(c). The recovered Fourier magnitude and zoomed in detail views of groups 2, 5, and 6 are shown in Fig. 6(e) and (f) respectively, showing faithful recovery of otherwise unresolved features.

Both the cost of assembling the camera array and the computational complexity of our reconstruction algorithm is  $O(N^2)$ . Therefore, minimizing the number of captured images necessary to recover each high resolution image is an important design criteria. There are two degrees of freedom to explore to help reduce the amount of ptychographic data acquired: changing the amount of overlap between neighboring images and changing the SAR.

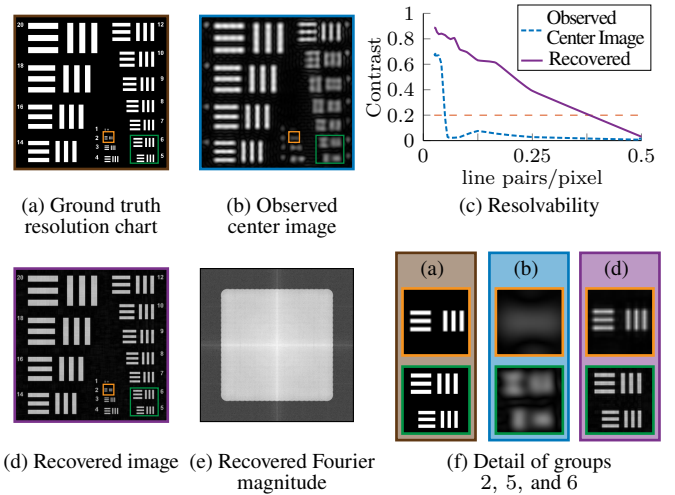


Fig. 6. **Recovering high frequency information using a Fourier ptychography.** (a) We simulate imaging a 64  $\times$  64 mm resolution target 50 meters away using sensor with a pixel pitch of 2  $\mu$ m. The width of a bar in group 20 is 2.5 mm. (b) The target is observed using a lens with a focal length of 800 mm and an aperture of 18 mm. The aperture is scanned over a  $21 \times 21$  grid (61% overlap) creating a synthetic aperture of 160 mm. The output of phase retrieval is a high resolution Fourier representation of the target. The recovered image is shown in (d) and the recovered Fourier magnitude (log scale) is shown in (e). The plot in (c) shows the contrast of the groups in the intensity images of the recovered resolution chart (purple solid line) and the observed center image (blue dashed line). Whereas the central image can only resolve elements which have a width of 12 pixels before contrast drops below 20%, using Fourier ptychography we are able to recover features which are only 2 pixels wide. Detail images of groups 2, 5, and 6, for the ground truth, observed, and recovered images are shown in (f).

### C. Effect of Overlap

Intuitively, increasing the amount of overlap should improve reconstruction performance. Redundant measurements help to constrain the reconstruction and provide some robustness to noise. In Fig. 7, we show the effects of increasing the amount of overlap from 0% (no overlap) to 77%, a large degree of overlap. The SAR is held constant at 10 for each overlap value, resulting in a  $9 \times 9$  sampling grid for 0% overlap and a much larger  $41 \times 41$  grid for 77% overlap. As seen in Fig. 7, the root-mean-squared error (RMSE) between the ground truth and recovered intensities decreases as the amount of overlap increases with a precipitous drop when the amount of overlap is greater than  $\sim 50\%$ . This watershed demarcates the boundary of recovering the high resolution image.

We can see the effect of varying the amount of overlap in the contrast plot and the recovered images shown in Fig. 7. Images captured with overlaps of 0% and 41% have large RMSE, fail to recover even low resolution features (even though the SAR is constant), and the resulting images are of low quality. Conversely, data captured with overlaps of 50% and 75% are able to reconstruct small features with low RMSE. Reconstruction quality also increases as the amount of overlap increases. Thus 50% is a lower bound on the amount of overlap required to run phase retrieval for an ideal imaging system [55], [25]. Additional overlap may be necessary for a real camera system. This observation coincides with previously reported overlap factors of 60% for good reconstruction [6].

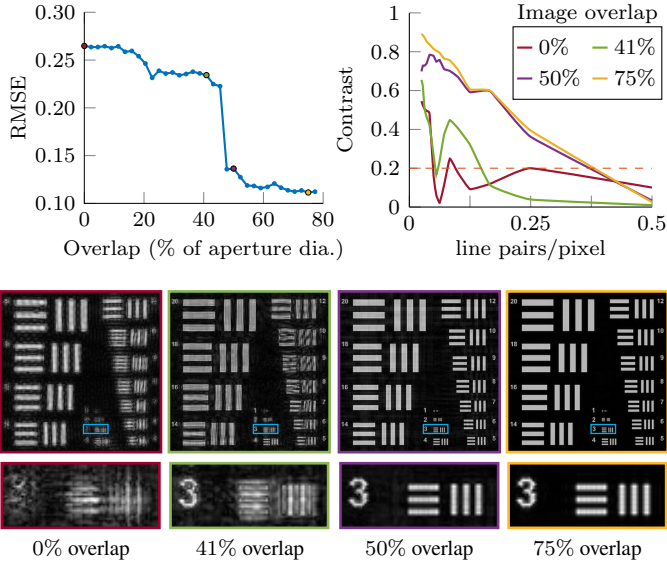


Fig. 7. **Effect of varying overlap between adjacent images.** Holding the synthetic aperture size constant, we vary the amount of overlap between adjacent images. As the amount of overlap increases, reconstruction quality improves. When the amount of overlap is less than 50%, we are unable to faithfully recover the high resolution image, as shown in the RMSE plot in the top left. The contrast plots of the intensity images for four selected overlap amounts (0%, 41%, 50%, and 75%) shows that insufficient overlap drastically reduces the resolution of the system. Recovered images show the increase in image reconstruction quality as the amount of overlap increases.

#### D. Effect of Synthetic Aperture Ratio (SAR)

Alternatively, the number of images may be reduced by decreasing the synthetic aperture ratio. For a given overlap, smaller SAR values will yield less improvement in resolution than larger SAR values (and a corresponding increase in the number of images). To demonstrate this, we use the same camera parameters as the previous experiment and fix overlap at 61% while varying the SAR. Fig. 8 shows that larger apertures can resolve smaller features, which can be clearly seen in the contrast plot. Without using ptychography, features less than 12 pixels wide (0.04 line pairs/pixel,  $25 \mu\text{m}$  at the image plane) cannot be resolved. Resolution steadily improves as the SAR increases to 5.64 before holding steady until an SAR of 11.8. As the SAR increases, image contrast also increases, which can be seen in the detail images shown in Fig. 8. Of course, increasing the SAR requires additional images; an SAR of 1.77 requires a  $3 \times 3$  sampling grid, while SARs of 3.32, 4.09, 5.64, and 11.8 require  $7 \times 7$ ,  $9 \times 9$ ,  $13 \times 13$ , and  $29 \times 29$  grids respectively. While, in theory, coherent camera arrays can improve resolution down to the wavelength of the illumination source, an order of magnitude in SAR requires a quadratic increase in the number of recorded images. Thus, the SAR should be set to the smallest size which meets the resolution requirement for a given application.

#### E. Effect of Noise on Image Recovery

The phase retrieval problem in (4) is non-convex and thus prone to getting stuck in local minima when using gradient descent procedures such as alternating minimization. Nonetheless, we observe that in practice our algorithm converges well for a variety of scenes and noise levels. We repeat the varying SAR experiment using the canonical Lena image, and with

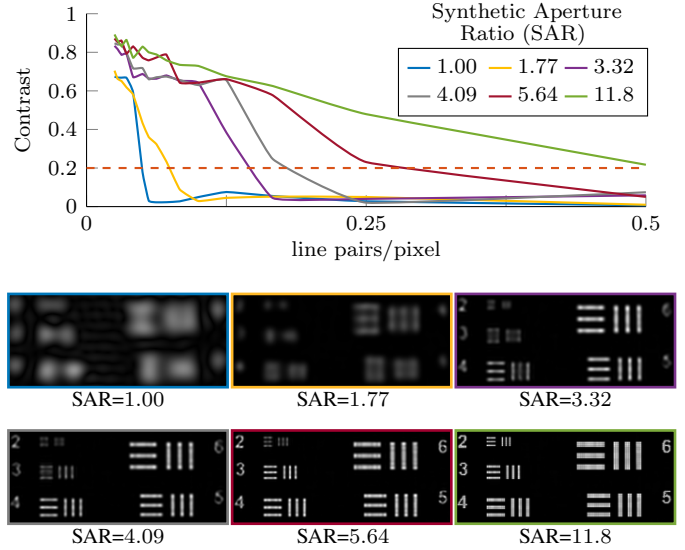


Fig. 8. **Varying synthetic aperture ratio (SAR).** For a fixed overlap of 61%, we vary the size of the synthetic aperture by adding cameras to array. As seen in the contrast plot of image intensities, as well as the reconstructed intensities below, the resolution of the recovered images increase as the SAR increases from 1 (the observed center image) to 11.8. We are able to recover group 2 with an SAR of 5.64, which requires 169 images.

varying levels of additive white Gaussian noise in the observed images. We test signal-to-noise ratios (SNR) of 10, 20, and 30 dB, and present the results in Fig. 9. Noise is added such that each captured image has the desired SNR. As shown in the RMSE plot, we are able to recover the high resolution image even with input images containing significant noise. The observed center images (SAR=1) reflect this noise, as well as diffraction blur, and thus exhibit a high RMS error. As the SAR increases, the resolution improves, the noise is suppressed, and the RMSE decreases (thanks to redundancy in the measurements). All remaining simulation experiments are conducted with an input SNR of 30 dB.

#### F. Comparison with Expensive Large Aperture Lenses

Next, we compare simulated images from an expensive and bulky lens, with simulated images from our coherent camera array. For these experiments we assume each system exhibits a fixed focal length of 1200 mm. In the early 1990s, Canon briefly made a 1200 mm lens with a 215 mm diameter aperture<sup>4</sup> which retailed for nearly \$150,000 US dollars (inflation adjusted to 2015) and weighed nearly 17 kilograms. At 30 meters, its minimum resolvable feature size is  $190 \mu\text{m}$  at the object plane (Nyquist-Shannon limit). This diffraction spot size is just small enough to recover the pertinent features of a fingerprint where the average ridge width is on the order of  $400 \mu\text{m}$  [48].

Instead of using such a large and expensive lens, one could alternatively consider imaging with a much smaller lens with 1200 mm focal length and a 75 mm diameter which may cost on the order of hundreds of dollars to manufacture. Such a lens would have a diffraction spot size of  $21 \mu\text{m}$  on the image sensor, and a minimum resolvable feature size

<sup>4</sup>Canon EF 1200mm  $f/5.6$ L USM

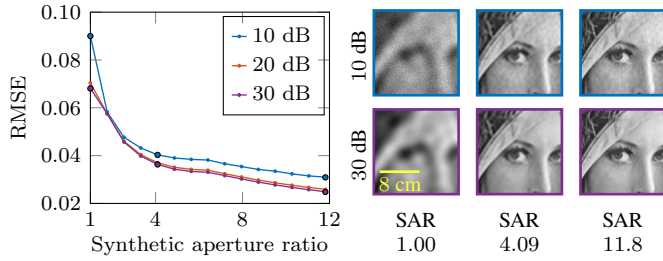


Fig. 9. **Noise robustness of the coherent camera array.** We repeat the experiment in Fig. 8 with the Lena image (assuming the scene is 650 meters away), while varying the amount of added Gaussian noise. The signal-to-noise ratio (SNR) of the input images is set to be 10, 20, and 30 dB. As shown in the RMSE plot, we are able to recover the high resolution image even with noisy input images. The observed center images (SAR=1) are blurry and noisy, with a high RMS error. As the SAR increases, the resolution improves, the noise is suppressed, and RMSE decreases. A cropped portion of select images are shown to highlight the performance of our approach. Note: all other simulation experiments are conducted with an input SNR of 30 dB.

of  $536 \mu\text{m}$  at 30 meters. The poor performance of this lens precludes identifying fingerprints directly from its raw images. However, incorporating such a lens into a coherent camera array, capturing multiple images, and reconstructing with ptychographic phase retrieval can offer a final diffraction-limited resolution that surpasses the large Canon lens.

We simulate imaging a fingerprint at 30 meters with both of the above approaches in Fig. 10. We use a fingerprint from the 2004 Fingerprint Verification Challenge [41] as ground truth, where each pixel corresponds to  $51 \mu\text{m}$  at the object plane, and the pixel size on the camera sensor is  $2 \mu\text{m}$  (as before). Using a 1200 mm focal length, 75 mm aperture lens with incoherent illumination yields images in which blur has degraded the image quality so that they are of no practical use (Fig. 10(a)). However, if the same lens is used to simulate an aperture diameter of 300 mm in a coherent camera array (61% overlap,  $9 \times 9$  images, SAR=4), the diffraction spot size reduces to  $130 \mu\text{m}$ , which is sufficient to identify the print, as shown in Fig. 10(b). The Canon lens with a 215 mm aperture could be used to achieve comparable quality, as in Fig. 10(c). Detail images in Fig. 10(d) highlight the image quality of the three imaging systems.

A similar experiment is conducted in Fig. 11 with the subject being a human face 1000 meters away. In this experiment, a synthetic aperture of 300 mm, corresponds to a diffraction spot size of 4.4 mm on the face. The 75 mm lens has a diffraction spot size of 180 mm and is again unable to resolve the scene with incoherent illumination but fine details are recovered using ptychography, Fig. 11(a) and (b) respectively. The Canon lens (Fig. 10(c)), yields a blurry image that is inferior to the image acquired under active illumination. Detailed crops of one of the eyes acquired using the three imaging setups are shown in Fig. 11(d).

While these simulations are limited in scope (i.e. we assume that diffraction is the only factor limiting resolution and neglect phase), the results suggest that implementing Fourier ptychography in a camera array offers a practical means to acquire high resolution images while remaining cost competitive with existing lenses. Moreover, such computational approaches appear as the only means available to surpass the resolution

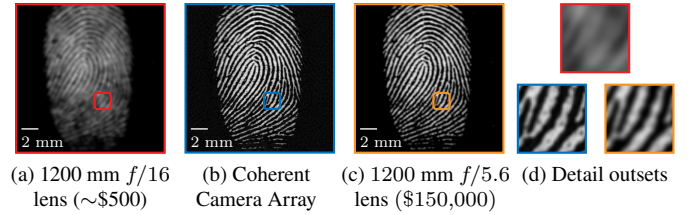


Fig. 10. **Simulation of imaging a fingerprint at 30 meters.** We simulate image capture with an inexpensive 1200 mm lens, 75 mm aperture diameter ( $f/16$ ), and a pixel pitch of  $2 \mu\text{m}$ . (a) Using passive illumination the resulting diffraction blur ( $530 \mu\text{m}$ ) removes details necessary to identify the fingerprint. (b) Imaging with a coherent camera array (61% overlap) that captures 81 images to create a synthetic aperture of 300 mm reduces diffraction blur to  $130 \mu\text{m}$ , and leads to faithful recovery of minutiae. (c) Using a \$150,000 lens with a 215 mm aperture diameter ( $f/5.6$ ), the diffraction blur reduces to  $190 \mu\text{m}$ , which is roughly comparable to our final reconstruction in (b). (d) Detail views of the three imaging systems. In this simulation diffraction is the only source of blur, other factors in TABLE I are not considered.

limits imposed by current manufacturing technology.

## VII. EXPERIMENTAL RESULTS

In this section, we experimentally verify our simulations of the coherent camera array. For simplicity, we use a transmissive setup similar to existing ptychography methods applied in microscopy. While this configuration is not practical for long distance imaging, we present the results as a proof-of-concept that we hope will directly extend to a reflection geometry. In Section VIII we discuss the practical limitations of implementing a long-range ptychography imaging system.

### A. Experimental Prototype

Our imaging system consists of a Blackfly machine vision camera manufactured by Point Grey (BFLY-PGE-50A2M-CS), coupled with a 75 mm Fujinon lens (HF75SA-1) that is mounted on a motorized 2D stage (VMX Bi-slide, see Fig. 12). For a single acquired data set, we scan over the synthetic aperture in a raster pattern. We discuss future geometries that avoid physical scanning in the next section. Objects to be imaged are placed 1.5 meters away from the camera and are illuminated with a helium neon (HeNe) laser which emits a beam with a wavelength of 633 nm. We employ a spatial filter to make the laser intensity more uniform as well as to ensure sufficient illumination coverage on our objects. A lens is placed immediately before the target to collect the illumination and form the Fourier transform on the aperture plane of the camera lens.

Lenses with small focal lengths can be easily (and cheaply) manufactured to have a proportionally large aperture. The maximum aperture of the lens that we use is 42 mm. In order to simulate building a cheap lens with a long focal length and small aperture, we stopped the lens down to  $f/32$ , creating a 2.3 mm diameter aperture. The diffraction spot size on the sensor is  $49 \mu\text{m}$  in diameter. Given that the camera sensor has a pixel width of  $2.2 \mu\text{m}$  we expect to see a blur of roughly 20 pixels.

Unique images are acquired by moving the camera to equidistant positions in the synthetic aperture plane via the translation stage. At every grid position, we capture multiple images with different exposures to form a high dynamic range reconstruction. By translating the camera, the shift in

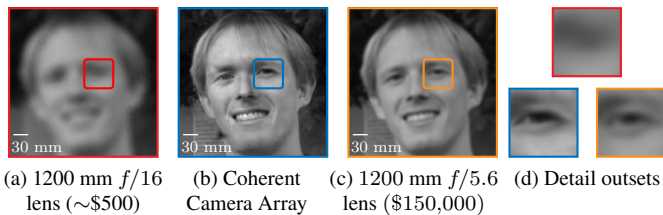


Fig. 11. **Simulation of capturing a face 1000 meters away.** We simulate image capture with an inexpensive 1200 mm lens, 75 mm aperture diameter ( $f/16$ ), and a pixel pitch of  $2 \mu\text{m}$ . (a) Directly using the inexpensive  $f/16$  lens in passive illumination results in a diffraction blur spot size of 17.8 mm on the face, obliterating detail necessary to recognize the subject. (b) Using Fourier ptychography (61% overlap, 81 images) to achieve a synthetic aperture of 300 mm the diffraction spot size is reduced to 4.4 mm. (c) Using the \$150,000 215 mm ( $f/5.6$ ) lens yields a diffraction spot size of 6.2 mm, 50% larger than the diffraction realized using Fourier ptychography. Detail views of the three systems are shown in (d). In this simulation diffraction is the only source of blur, other factors in TABLE I are not considered.

perspective causes the captured images to be misaligned. For planar scenes a pair of misaligned images can be corrected by finding the homography relating the reference viewpoint (taken to be the center position) and the outlying view. We accomplish this by finding fiducial markers of a checkerboard pattern affixed to the object, which is lit with incoherent light. The translation stage is of high enough precision to allow the calibration step to be performed immediately before or after data capture. The aligned high dynamic range images are used as inputs to the phase retrieval algorithm.

### B. Recovered images

We test our setup with three scenes. First, we deposit a fingerprint on a glass microscope slide and use consumer grade fingerprint powder to reveal the latent print. Our second scene contains a translucent water bottle label, and our third scene is a resolution target. For the scenes containing the fingerprint and water bottle labels, we record a  $17 \times 17$  grid of images with 81% overlap between adjacent images, resulting in a synthetic aperture with a 9.3 mm diameter ( $\text{SAR}=4$ ).

**Fingerprint:** Fig. 13 shows the results of using our coherent camera array prototype to improve the resolution of a fingerprint. With an aperture diameter of 2.3 mm, little high spatial frequency information is transferred to the image plane in a single image, resulting in the blurry image in Fig. 13(a). The coherent camera array technique recovers a high resolution Fourier representation of the object, from which we recover both the high resolution image and the phase of the object (Fig. 13(b)). The wrapping in the recovered phase could be caused by the illumination wavefront, or by a tilt in the object with respect to the camera. One consequence of stopping down the lens aperture is that we are able to fully open the aperture and record an image which does not exhibit any diffraction blur, Fig. 13(c), which provides a useful comparison for our reconstruction. Detail views of the three imaging scenarios are shown in Fig. 13(d).

**Dasani label:** We next use the same setup to capture a translucent Dasani water bottle label, shown in Fig. 14. Unlike the fingerprint, the diffuse water bottle label has a random phase which produces a highly varying optical field at the

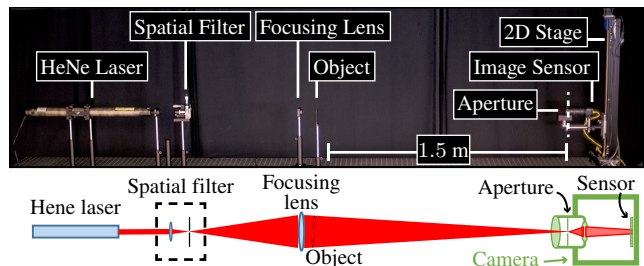


Fig. 12. **Overview of hardware configuration for data acquisition (side view).** From left to right: A helium neon laser passed through a spatial filter acts as the coherent illumination source. A focusing lens forms the Fourier transform of the transmissive object at the aperture plane of the camera's lens. The aperture acts as a bandpass filter of the Fourier transform and the signal undergoes an inverse Fourier transform as it is focused onto the camera's sensor. The camera (Point Grey Blackfly (BFLY-PGE-50A2M-CS) is mounted on a motorized 2D stage to capture overlapping images.

image plane, which is reminiscent of laser speckle. Speckle becomes more pronounced for small apertures (Fig. 14(a)). The recovered image in Fig. 14(b) shows that the coherent camera array can recover details that are completely lost in a diffraction limited system, and the phase retrieval algorithm is able to handle the quickly varying random phase of the label. Even with a modest increase to the SAR, individual letters are legible, as highlighted in the detailed crops in Fig. 14(d). If we were to further increase the SAR, we could further reduce speckle-induced artifacts, as suggested by the raw open-aperture image in Fig. 14(c).

**USAF target:** We use the same setup to capture a USAF target, but now with a different 75 mm lens (Edmund Optics #54-691) and a slightly different Blackfly camera (BFLY-PGE-13S2M-CS) with a pixel pitch of  $3.75 \mu\text{m}$ . Using this setup, and an aperture diameter of 2.5 mm, we expect a diffraction blur size of  $48 \mu\text{m}$  on the image sensor (approximately 12 sensor pixels). With the USAF target placed 1.5 meters away from the camera, we expect a diffraction blur size of  $970 \mu\text{m}$  at the object plane. We observe that the resolution of the USAF target is limited to 1.26 line pairs per millimeter (lp/mm) in the center observed image (Group 0, Element 3 in Fig. 15a). By acquiring a  $23 \times 23$  grid of images, with 72% overlap between neighboring images, we achieve an effective synthetic aperture ratio of 7.16. We show the results of such a coherent camera array reconstruction in Fig. 15(b), where the spatial recovered spatial resolution has increased to 8.98 lp/mm (Group 3, Element 2), a  $7.12 \times$  improvement in resolution.

As discussed in Section VI, varying the synthetic aperture ratio impacts the system resolution enhancement factor. This can be observed by varying the number of images used to recover the USAF target. In Fig. 15(c) we present two regions of the target for a varying SAR of 1 – 7.16. As the SAR increases to 2.12, 4.36, 5.48, and 7.16 the realized resolution gains are 1.94, 4.00, 5.66, and 7.12 respectively, which closely tracks the expected behavior.

**Reproducible Research:** We are committed to reproducible research. Our codes and data sets may be found on our project webpage [27] (<http://jrholloway.com/projects/towardCCA>).

## VIII. BARRIERS TO BUILDING A REAL SYSTEM

In this section we discuss potential barriers to implementing a coherent camera array for long range imaging. Where

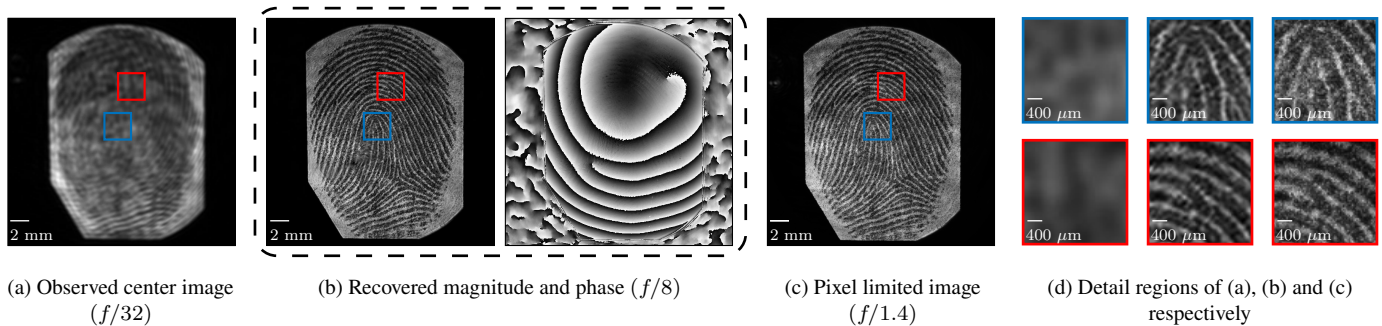


Fig. 13. **Experimental result: Resolving a fingerprint  $4\times$  beyond the diffraction limit.** Using the hardware setup shown in Fig. 12, we use a 75 mm focal length lens to acquire images of a fingerprint  $\sim 1.5$  m away from the camera. A fingerprint was pressed on a glass slide and fingerprint powder was used to make the ridges opaque. (a) Stopping down the aperture to a diameter of 2.34 mm induces a diffraction spot size of  $49 \mu\text{m}$  on the sensor ( $\sim 20$  pixels) and  $990 \mu\text{m}$  on the object. (b) We record a grid of  $17 \times 17$  images with an overlap of 81%, resulting in a SAR which is 4 times larger than the lens aperture. After running phase retrieval, we recover a high resolution magnitude image and the phase of the objects. (c) For comparison, we open the aperture to a diameter of 41 mm to reduce the diffraction blur to the size of a pixel. (d) Comparing zoomed in regions of the observed, recovered, and comparison images shows that our framework is able to recover details which are completely lost in a diffraction limited system.

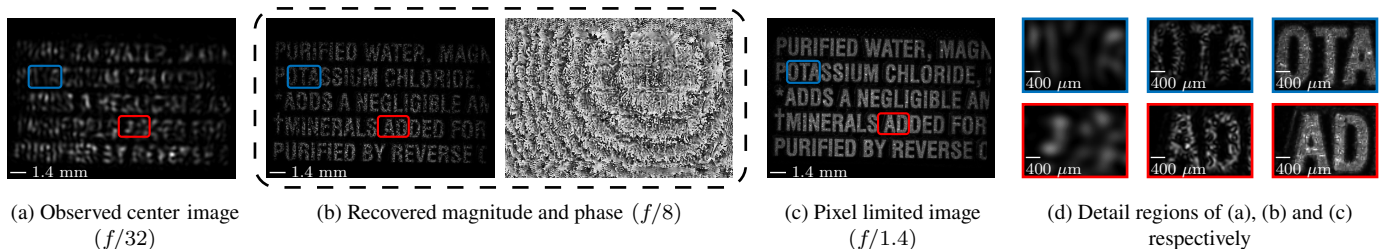


Fig. 14. **Experimental result: Resolving  $4\times$  beyond the diffraction limit for a diffuse water bottle label.** Using the same parameters as in Fig. 13, we image a diffuse water bottle label  $\sim 1.5$  m away from the camera. The diffuse nature of the water bottle label results in laser speckle. In the observed center image (a), diffraction blur and laser speckle render the text illegible. Using Fourier ptychography (b) we are able to reduce the effect of speckle and remove diffraction revealing the text. In the comparison image (c) the text is clearly legible. Detail views in (d) show the improvement in image resolution when using Fourier ptychography.

possible, we present preliminary simulation results.

**Single-shot imaging:** One limitation of the ptychography framework with a single camera and illumination source is that it assumes a static or a slow-moving scene. This restriction arises because, in order to sample a large Fourier space, we capture images while moving the camera one step at a time.

To enable imaging dynamic scenes, we envision a design with multiple cameras and illumination sources that can sample a large Fourier space in a *single shot*. We illustrate the modified design in Fig. 16, where we consider an array of cameras in a tightly packed configuration and an array of illumination sources that are placed such that the optical fields generated by them at the aperture plane are slightly shifted with respect to one another.

By changing the location and angle of the illumination source, we can shift the optical field at the aperture plane. Therefore, if we use multiple illumination sources at once, they will produce multiple, shifted optical fields at the aperture plane. In such a multiplexed illumination setting, each camera in the array samples multiple, shifted copies of a reference Fourier plane. The sampling pattern is determined by the relative positions and orientations of the cameras and the illumination sources. Since the illumination sources are incoherent with each other, the intensity image measured at each camera corresponds to the sum of intensities from different Fourier regions. Furthermore, we can also capture multiple images by changing the illumination pattern. Similar

multiplexed illumination methods have already been used for high-resolution microscopy in [60].

Suppose our system consists of  $P$  cameras and  $Q$  illumination sources that divide the Fourier space into overlapping apertures with centers  $(c_{x'_i}, c_{y'_i})$ , where  $i$  indicates a camera-illumination source pair. Suppose we capture  $T$  images while changing the illumination patterns. Let us describe the images measured by camera  $p \in \{1, \dots, P\}$  with the  $t$ th illumination pattern as follows

$$I_{p,t} = \sum_{i \in \mathcal{M}(p,t)} |\mathcal{F}\mathcal{R}_{\Omega_i}\hat{\psi}|^2, \quad (7)$$

where  $\mathcal{M}(p,t)$  denotes the indices for those apertures in the Fourier plane that are multiplexed in the recorded image  $I_{p,t}$ .  $\hat{\psi}$  denotes the complex-valued field at the aperture plane and  $\mathcal{R}_{\Omega_i}\hat{\psi}$  denotes an aperture operator that only selects the entries of  $\hat{\psi}$  inside the set  $\Omega_i$ . To recover the high-resolution  $\hat{\psi}$  from a sequence of  $P * T$  multiplexed, low-resolution, intensity measurements,  $\{I_{p,t}\}$ , we use an alternating minimization-based phase retrieval problem similar to the one depicted in Figure 5, where we iteratively estimate the complex-valued field at the sensor planes:  $\psi_i^k = \mathcal{F}\mathcal{R}_{\Omega_i}\hat{\psi}$ . The only change appears in enforcing the magnitude constraints, where we replace the magnitudes of  $\psi_i^k$  at  $k$ th iteration as follows,

$$\psi_i^k \leftarrow \sqrt{\frac{I_{k,t}}{\sum_{i \in \mathcal{M}(k,t)} |\psi_i^k|^2}} \psi_i^k \quad \text{for all } i \in \mathcal{M}(p,t). \quad (8)$$

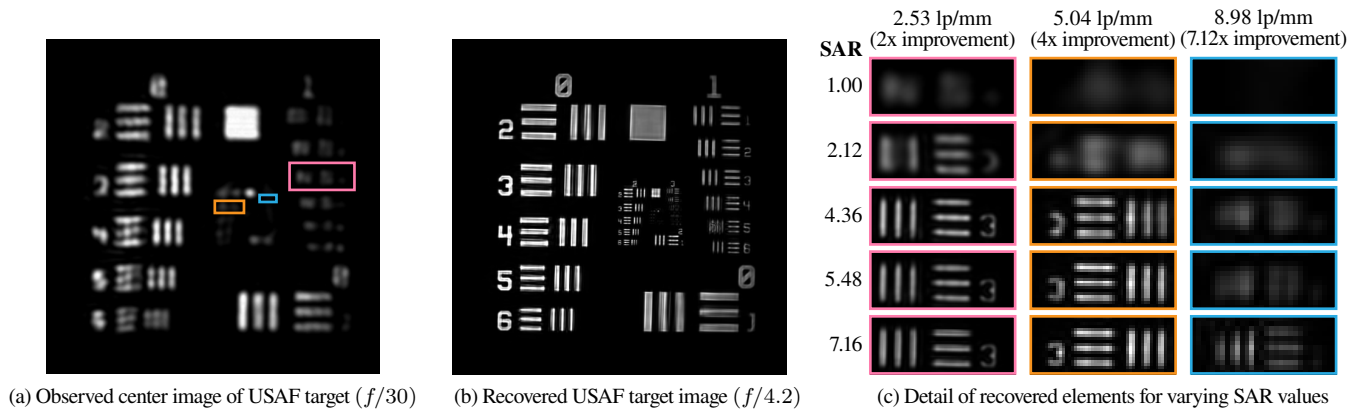


Fig. 15. **Experimental result: Recovering a USAF target with varying SAR.** We capture a USAF resolution target 1.5 meters away from the camera. For this experiment, we use a slightly different lens and image sensor (focal length = 75 mm, pixel pitch =  $3.75 \mu\text{m}$ ). (a) The camera is stopped down to 2.5 mm which induces a  $930 \mu\text{m}$  blur on the resolution chart, limiting resolution to 1.26 line pairs per millimeter (lp/mm). (b) We record a  $23 \times 23$  grid of images with 72% overlap, resulting in a SAR of 7.16. Following phase retrieval, we are able to resolve features as small as 8.98 lp/mm, a  $7.12\times$  improvement in resolution. (c) We show the effect of varying the SAR on resolution. Using a subset of the captured images we vary the SAR from 2.12 up to 7.16. The gains in improvement closely track the SAR.

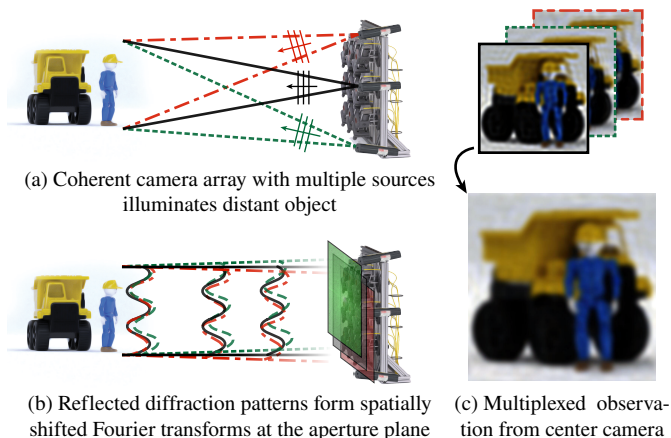


Fig. 16. **An illustration of ptychography with multiplexed illumination and a camera array.**(a) Multiple coherent sources illuminate a distant scene. (Note: different colors are used to distinguish light sources; however, we assume each source operates in the same wavelength.) (b) Reflected light undergoes Fraunhofer diffraction forming spatially shifted Fourier transforms at the aperture plane of the camera array. (c) A single camera aperture (e.g. center camera) sums the intensities from each diffraction pattern (top), recording a single image (bottom).

To gauge the potential of the multiplexed illumination scheme, we simulate the recovery of a resolution chart using a  $7 \times 7$  camera array. Cameras are positioned in a square grid such that their lenses abut; each camera effectively samples a non-overlapping region of the Fourier plane. Every camera is assumed to have a lens with an 800 mm focal length, and an aperture limited by the front lens diameter of 25 mm. The resolution chart ( $64 \text{ mm} \times 64 \text{ mm}$ ) is placed 50 meters away, and assuming a light source with a wavelength of 550 nm and a pixel pitch of  $2 \mu\text{m}$ , the diffraction spot size is  $\approx 20$  pixels. We use a  $7 \times 7$  array of illumination sources adjusted so that they provide 66% overlap between adjacent apertures in the Fourier plane.

We present the results in Fig. 17, where we examine the effects of increasing the number of active illumination sources per image ( $N_{\text{mux}}$ ) and the number of images captured with

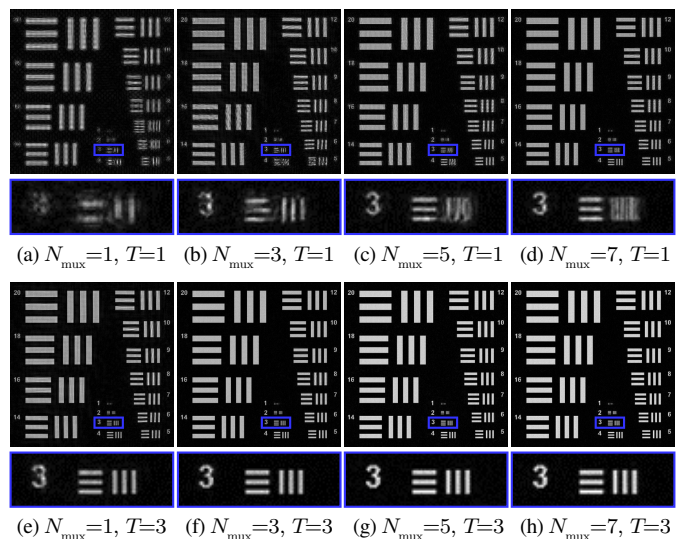


Fig. 17. **Simulation of recovering a resolution target using multiplexed illumination patterns.** We repeat the conditions of Fig. 6 using a  $7 \times 7$  camera array. Each camera has an 800 mm lens with an aperture (front lens diameter) of 25 mm. Cameras are placed such that their apertures abut, though don't overlap, in the Fourier plane. Illumination sources provide 66% overlap among neighboring apertures in the Fourier plane.  $N_{\text{mux}}, T$  in subcaptions denote the number of active illumination sources per image ( $N_{\text{mux}}$ ) and the number of images captured with different illumination patterns ( $T$ ), respectively. Recovered images show that increasing  $N_{\text{mux}}$  and  $T$  improves the quality of the reconstructed images.

different illumination patterns ( $T$ ). We recorded multiplexed images under different illumination patterns according to the model in (7). In each experiment, we recorded  $T$  images by randomly selecting a different  $N_{\text{mux}}$  active illumination sources from the  $7 \times 7$  lighting array for every image. We recovered the resolution target using the algorithm described in Fig. 5 along with the modification in (8). The sampling scheme with  $N_{\text{mux}} = 1, T = 1$  (i.e. ptychography with 0% overlap) leaves holes in the Fourier plane; therefore, the reconstruction shows severe aliasing artifacts. As we increase  $N_{\text{mux}}$ , the sampling space fills up the entire Fourier plane and also introduces overlaps in the observed measurements, which

improves the reconstruction quality. Fig. 17(a)–17(d) show the results for single-shot imaging ( $T = 1$ ) with increasing number of active illumination sources per image. The quality of reconstruction significantly improves if we capture multiple images with the camera array. Fig. 17(e)–17(h) show the images recovered from  $T = 3$  sets of images, each captured with a different pattern of  $N_{\text{mux}}$  active illumination sources. These results indicate that combining a camera array with an array of programmable illumination sources can help us design a single- or multi-shot imaging system that can potentially capture real-world, dynamic scenes.

**Diffuse Materials:** Diffuse objects are materials which have a rough surface at the scale of illumination wavelength. The randomness in the surface manifests as a rapidly changing random phase for the object. In Fig. 14, we presented results for a diffuse water bottle label which exhibited significant laser speckle due to the random phase of the label. We were able to recover the high-resolution magnitude and phase. While this material was weakly diffuse, it suggests that it should be possible to use Fourier ptychography to improve resolution of everyday objects in long distance images. Characterizing the performance of FP for diffuse objects is a subject of future research.

**Reflective Recovery:** Traditionally, ptychography has been restricted to working in a transmissive modality. This arrangement is impractical in long range imaging, if one can get close enough to position a laser to shine through an object then they can snap a picture. Recent work suggests that Fourier ptychography can be extended to work in reflective mode [50], though more research is needed to characterize the performance and confirm it as a viable technique for long distance imaging.

## IX. CONCLUSION

In this paper we have proposed using Fourier ptychography to dramatically improve resolution in long distance imaging. Whereas existing super-resolution techniques only offer a  $2\times$  improvement in resolution, the gains in ptychography are (theoretically) orders of magnitude greater. We have demonstrated resolution gains of  $7.12\times$  for real scenes and show simulation results with  $10\times$  improvement in resolution.

One consideration which must be addressed before realizing a long-distance ptychographic system is how to account for dynamic scenes. In the current system, a camera is affixed to a translation stage and images are acquired sequentially over the course of tens of minutes. We have proposed using an array of cameras fitted with inexpensive lenses and multiplexed illumination to capture images simultaneously, a necessary requirement for capturing dynamic scenes. A greater concern is implementing a ptychographic system in reflective mode. It is impractical to position a laser source behind an object to be imaged remotely, which necessitates the placement of the illumination source near to the image sensor. We believe our initial results show great promise that a practical reflective mode ptychography system can be implemented for imaging long distances. In the future, we plan to design, build, and test such camera array systems as an extension of the work presented here.

## ACKNOWLEDGMENT

This work was supported in part by NSF grants IIS-1116718, CCF-1117939, CCF-1527501, NSF CAREER grant IIS-1453192, ONR grant 1(GG010550)/N00014-14-1-0741, and a Northwestern University McCormick Catalyst grant. The authors would also like to thank Richard Baranuik and Aggelos Katsaggelos for their fruitful discussions and comments.

## REFERENCES

- [1] S. Baker and T. Kanade. Limits on Super-resolution and How to Break Them. *Pattern Analysis and Machine Intelligence, IEEE Transactions on*, 24(9):1167–1183, 2002.
- [2] S. Baker, T. Sim, and T. Kanade. When is the Shape of a Scene Unique Given Its Light-Field: A Fundamental Theorem of 3D Vision? *Pattern Analysis and Machine Intelligence, IEEE Transactions on*, 25(1):100–109, 2003.
- [3] M. J. Booth. Adaptive Optics in Microscopy. *Philosophical Transactions of the Royal Society of London A: Mathematical, Physical and Engineering Sciences*, 365(1861):2829–2843, 2007.
- [4] S. Borman and R. Stevenson. Spatial Resolution Enhancement of Low-resolution Image Sequences-A Comprehensive Review With Directions for Future Research. *Lab. Image and Signal Analysis, University of Notre Dame, Tech. Rep.*, 1998.
- [5] M. Born and E. Wolf. *Principles of Optics: Electromagnetic Theory of Propagation, Interference and Diffraction of Light*. CUP Archive, 2000.
- [6] O. Bunk, M. Dierolf, S. Kynde, I. Johnson, O. Marti, and F. Pfeiffer. Influence of the Overlap Parameter on the Convergence of the Ptychographical Iterative Engine. *Ultramicroscopy*, 108(5):481–487, 2008.
- [7] G. Carles, J. Downing, and A. R. Harvey. Super-Resolution Imaging Using a Camera Array. *Optics Letters*, 39(7):1889–1892, 2014.
- [8] K. Dabov, A. Foi, V. Katkovich, and K. Egiazarian. Image Denoising by Sparse 3-D Transform-domain Collaborative Filtering. *Image Processing, IEEE Transactions on*, 16(8):2080–2095, 2007.
- [9] R. F. Dantowitz, S. W. Teare, and M. J. Kozubal. Ground-based High-resolution Imaging of Mercury. *The Astronomical Journal*, 119(5):2455, 2000.
- [10] S. Dong, R. Horstmeyer, R. Shiradkar, K. Guo, X. Ou, Z. Bian, H. Xin, and G. Zheng. Aperture-Scanning Fourier Ptychography for 3D Refocusing and Super-resolution Macroscopic Imaging. *Optics Express*, 22(11):13586–13599, 2014.
- [11] S. Dong, R. Shiradkar, P. Nanda, and G. Zheng. Spectral Multiplexing and Coherent-State Decomposition in Fourier Ptychographic Imaging. *Biomedical Optics Express*, 5(6):1757, 2014.
- [12] T. Edo, D. Batey, A. Maiden, C. Rau, U. Wagner, Z. Pešić, T. Waigh, and J. Rodenburg. Sampling in X-Ray Ptychography. *Physical Review A*, 87(5):053850, 2013.
- [13] B. L. Ellerbroek. First-order Performance Evaluation of Adaptive-optics Systems for Atmospheric-turbulence Compensation in Extended-Field-of-View Astronomical Telescopes. *JOSA A*, 11(2):783–805, 1994.
- [14] V. Elser. Phase Retrieval by Iterated Projections. *JOSA A*, 20(1):40–55, 2003.
- [15] J. Fienup and C. Wackerman. Phase-Retrieval Stagnation Problems and Solutions. *JOSA A*, 3(11):1897–1907, 1986.
- [16] J. R. Fienup. Phase Retrieval Algorithms: A Comparison. *Applied Optics*, 21(15):2758–2769, 1982.
- [17] W. T. Freeman, T. R. Jones, and E. C. Pasztor. Example-based Super-resolution. *Computer Graphics and Applications, IEEE*, 22(2):56–65, 2002.
- [18] D. L. Fried. Probability of Getting a Lucky Short-Exposure Image Through Turbulence. *JOSA*, 68(12):1651–1657, 1978.
- [19] A. Fruchter and R. Hook. Drizzle: A Method for the Linear Reconstruction of Undersampled Images. *Publications of the Astronomical Society of the Pacific*, 114(792):144–152, 2002.
- [20] R. Gerchberg. Super-resolution Through Error Energy Reduction. *Journal of Modern Optics*, 21(9):709–720, 1974.
- [21] R. W. Gerchberg. A Practical Algorithm for the Determination of Phase From Image and Diffraction Plane Pictures. *Optik*, 35:237, 1972.
- [22] D. Glasner, S. Bagon, and M. Irani. Super-resolution From a Single Image. In *Computer Vision, 2009 IEEE 12th International Conference on*, pages 349–356. IEEE, 2009.
- [23] K. Guo, S. Dong, P. Nanda, and G. Zheng. Optimization of Sampling Pattern and the Design of Fourier Ptychographic Illuminator. *Optics Express*, 23(5):6171–6180, 2015.
- [24] T. Harada, M. Nakasuji, Y. Nagata, T. Watanabe, and H. Kinoshita. Phase Imaging of Extreme-Ultraviolet Mask Using Coherent Extreme-Ultraviolet Scatterometry Microscope. *Japanese Journal of Applied Physics*, 52(6S):06GB02, 2013.

- [25] T. Heinosaaari, L. Mazzarella, and M. M. Wolf. Quantum Tomography Under Prior Information. *Communications in Mathematical Physics*, 318(2):355–374, 2013.
- [26] T. R. Hillman, T. Gutzler, S. A. Alexandrov, and D. D. Sampson. High-resolution, Wide-field Object Reconstruction With Synthetic Aperture Fourier Holographic Optical Microscopy. *Optics Express*, 17(10):7873–7892, 2009.
- [27] J. Holloway, M. S. Asif, M. K. Sharma, N. Matsuda, R. Horstmeyer, O. Cossairt, and A. Veeraraghavan. Project Webpage, October 2015. <http://jrholloway.com/projects/towardCCA>.
- [28] J. Holloway, A. C. Sankaranarayanan, A. Veeraraghavan, and S. Tambe. Flutter Shutter Video Camera for Compressive Sensing of Videos. In *Computational Photography (ICCP), 2012 IEEE International Conference on*, pages 1–9. IEEE, 2012.
- [29] R. Horstmeyer, R. Y. Chen, X. Ou, B. Ames, J. A. Tropp, and C. Yang. Solving Ptychography with a Convex Relaxation. *New Journal of Physics*, 17(053004):1–15, 2015.
- [30] R. Horstmeyer, X. Ou, J. Chung, G. Zheng, and C. Yang. Overlapped Fourier Coding for Optical Aberration Removal. *Optics Express*, 22(20):24062–24080, 2014.
- [31] N. Joshi and M. F. Cohen. Seeing Mt. Rainier: Lucky Imaging for Multi-image Denoising, Sharpening, and Haze Removal. In *Computational Photography (ICCP), 2010 IEEE International Conference on*, pages 1–8. IEEE, 2010.
- [32] S. B. Kang. Automatic Removal of Chromatic Aberration from a Single Image. In *Computer Vision and Pattern Recognition, 2007. CVPR'07. IEEE Conference on*, pages 1–8. IEEE, 2007.
- [33] K. T. Knox and B. J. Thompson. Recovery of Images From Atmospherically Degraded Short-Exposure Photographs. *The Astrophysical Journal*, 193:L45–L48, 1974.
- [34] A. Labeyrie. Attainment of Diffraction Limited Resolution in Large Telescopes by Fourier Analysing Speckle Patterns in Star Images. *Astronomy & Astrophysics*, 6(1):85–87, 1970.
- [35] A. Levin, P. Sand, T. S. Cho, F. Durand, and W. T. Freeman. Motion-Invariant Photography. *ACM Transactions on Graphics (TOG)*, 27(3):71, 2008.
- [36] P. Li, D. J. Batey, T. B. Edo, and J. M. Rodenburg. Separation of Three-Dimensional Scattering Effects in Tilt-Series Fourier Ptychography. *Ultramicroscopy*, 158:1–7, 2015.
- [37] Z. Lin and H.-Y. Shum. Fundamental Limits of Reconstruction-based Superresolution Algorithms Under Local Translation. *Pattern Analysis and Machine Intelligence, IEEE Transactions on*, 26(1):83–97, 2004.
- [38] A. W. Lohmann. Scaling Laws for Lens Systems. *Applied Optics*, 28(23):4996–4998, 1989.
- [39] A. W. Lohmann, G. Weigelt, and B. Winitzer. Speckle Masking in Astronomy: Triple Correlation Theory and Applications. *Applied Optics*, 22(24):4028–4037, 1983.
- [40] A. M. Maiden and J. M. Rodenburg. An Improved Ptychographical Phase Retrieval Algorithm for Diffractive Imaging. *Ultramicroscopy*, 109(10):1256–1262, 2009.
- [41] D. Maltoni, D. Maio, A. K. Jain, and S. Prabhakar. *Handbook of Fingerprint Recognition*. Springer Science & Business Media, 2009.
- [42] L. Martínez-León and B. Javidi. Synthetic Aperture Single-Exposure On-Axis Digital Holography. *Optics Express*, 16(1):161–169, 2008.
- [43] J. H. Massig. Digital Off-Axis Holography With a Synthetic Aperture. *Optics Letters*, 27(24):2179–2181, 2002.
- [44] R. D. McClure, W. A. Grundmann, W. N. Rambold, J. M. Fletcher, E. H. Richardson, J. R. STILBURN, R. Racine, C. A. Christian, and P. Waddell. An Image-Stabilization, High-resolution Camera for the Canada-France-Hawaii Telescope. *Publications of the Astronomical Society of the Pacific*, pages 1156–1165, 1989.
- [45] V. Mico, Z. Zalevsky, P. García-Martínez, and J. García. Synthetic Aperture Superresolution With Multiple Off-Axis Holograms. *JOSA A*, 23(12):3162–3170, 2006.
- [46] P. Milanfar, editor. *Super-Resolution Imaging*. CRC Press, 2010.
- [47] K. Nasrollahi and T. B. Moeslund. Super-resolution: A Comprehensive Survey. *Machine Vision and Applications*, 25(6):1423–1468, 2014.
- [48] T. Orczyk and L. Wieclaw. Fingerprint Ridges Frequency. In *Nature and Biologically Inspired Computing (NaBIC), 2011 Third World Congress on*, pages 558–561. IEEE, 2011.
- [49] X. Ou, G. Zheng, and C. Yang. Embedded Pupil Function Recovery for Fourier Ptychographic Microscopy. *Optics Express*, 22(5):4960–4972, 2014.
- [50] S. Pacheco, B. Salahieh, T. Milster, J. J. Rodriguez, and R. Liang. Transfer Function Analysis in Epi-illumination Fourier Ptychography. *Optics Letters*, preprint, 2015.
- [51] A. Papoulis. A New Algorithm in Spectral Analysis and Band-Limited Extrapolation. *Circuits and Systems, IEEE Transactions on*, 22(9):735–742, 1975.
- [52] T. Q. Pham, L. J. Van Vliet, and K. Schutte. Robust Fusion of Irregularly Sampled Data Using Adaptive Normalized Convolution. *EURASIP Journal on Advances in Signal Processing*, 2006(1):1–12, 2006.
- [53] R. Raskar, A. Agrawal, and J. Tumblin. Coded Exposure Photography: Motion Deblurring Using Fluttered Shutter. *ACM Transactions on Graphics (TOG)*, 25(3):795–804, 2006.
- [54] M. C. Roggemann, B. M. Welsh, and B. R. Hunt. *Imaging Through Turbulence*. CRC press, 1996.
- [55] P. Schniter and S. Rangan. Compressive Phase Retrieval Via Generalized Approximate Message Passing. *Signal Processing, IEEE Transactions on*, 63(4):1043–1055, 2015.
- [56] C. J. Schuler, M. Hirsch, S. Harmeling, and B. Schölkopf. Non-stationary Correction of Optical Aberrations. In *Computer Vision (ICCV), 2011 IEEE International Conference on*, pages 659–666. IEEE, 2011.
- [57] M. D. Seaberg, B. Zhang, D. F. Gardner, E. R. Shanblatt, M. M. Murnane, H. C. Kapteyn, and D. E. Adams. Tabletop nanometer extreme ultraviolet imaging in an extended reflection mode using coherent Fresnel ptychography. *Optica*, 1(1):39–44, 2014.
- [58] T. A. ten Brummelaar, H. A. McAlister, S. T. Ridgway, J. W. G. Baguolo, N. H. Turner, L. Sturmman, J. Sturmman, D. H. Berger, C. E. Ogden, R. Cadman, W. I. Hartkopf, C. H. Hopper, and M. A. Shure. First Results From the CHARA Array. II. A Description of the Instrument. *The Astrophysical Journal*, 628(1):453, 2005.
- [59] P. Thibault, M. Dierolf, A. Menzel, O. Bunk, C. David, and F. Pfeiffer. High-Resolution Scanning X-Ray Diffraction Microscopy. *Science*, 321(5887):379–382, 2008.
- [60] L. Tian, X. Li, K. Ramchandran, and L. Waller. Multiplexed Coded Illumination for Fourier Ptychography with an LED Array Microscope. *Biomedical Optics Express*, 5(7):2376–2389, 2014.
- [61] L. Tian and L. Waller. 3D Intensity and Phase Imaging From Light Field Measurements in an LED Array Microscope. *Optica*, 2(2):104–111, 2015.
- [62] P. Vandewalle, S. Süsstrunk, and M. Vetterli. A Frequency Domain Approach to Registration of Aliased Images with Application to Super-Resolution. *EURASIP Journal on Applied Signal Processing (special issue on Super-resolution)*, 2006:Article ID 71459, 14 pages, 2006.
- [63] K. Venkataraman, D. Lelescu, J. Duparré, A. McMahon, G. Molina, P. Chatterjee, R. Mullis, and S. Nayar. PiCam: An Ultra-Thin High Performance Monolithic Camera Array. *ACM Transactions on Graphics (TOG)*, 32(6):166, 2013.
- [64] P. Walkenhorst. World’s Most Expensive Camera Lens, April 2012. <http://www.apotelyt.com/photo-lens/leica-most-expensive-lens>.
- [65] B. Wilburn, N. Joshi, V. Vaish, E.-V. Talvala, E. Antunez, A. Barth, A. Adams, M. Horowitz, and M. Levoy. High Performance Imaging Using Large Camera Arrays. *ACM Transactions on Graphics (TOG)*, 24(3):765–776, 2005.
- [66] S. Zhang, J. Zhao, and J. Wang. An Efficient Lucky Imaging System for Astronomical Image Restoration. In *Advanced Maui Optical and Space Surveillance Technologies Conference; 754-761, Advanced Maui Optical and Space Surveillance Technologies*, 2011.
- [67] G. Zheng, R. Horstmeyer, and C. Yang. Wide-field, High-resolution Fourier Ptychographic Microscopy. *Nature Photonics*, 7(9):739–745, 2013.
- [68] A. Zomet, A. Rav-Acha, and S. Peleg. Robust Super-Resolution. In *Computer Vision and Pattern Recognition, 2001. CVPR 2001. Proceedings of the 2001 IEEE Computer Society Conference on*, volume 1, pages 1–645. IEEE, 2001.



**Jason Holloway** is a Ph.D. candidate working under the guidance of Ashok Veeraraghavan in the Electrical and Computer Engineering department of Rice University. His research interests are in computational imaging & photography and computer vision. He earned his B.S. degrees in Electrical and Computer Engineering and Physics from Clarkson University in 2010 and his M.S. in Electrical and Computer Engineering from Rice University in 2013.



**Salman Asif** is a Postdoctoral Scholar in the Department of Electrical and Computer Engineering at Rice University. Dr. Asif received his B.Sc. degree in 2004 from the University of Engineering and Technology, Lahore, Pakistan, and an M.S.E.E degree in 2008 and a Ph.D. degree in 2013 from the Georgia Institute of Technology, Atlanta, Georgia. His research interests include compressive sensing, computational and medical imaging, and machine learning.



**Roarke Horstmeyer** is currently an Einstein International Postdoctoral Fellow at Charité Medical University in Berlin, Germany. He recently received his PhD from the Electrical Engineering department at Caltech, where he was a member of the Biophotonics Lab. Roarke received a Masters degree from the MIT Media Lab and a BS degree in Physics and Japanese from Duke University. His primary research interests include computational optics, wavefront shaping, and techniques to image deep into tissue.



**Manoj K. Sharma** is a Postdoctoral Scholar with the Department of Electrical and Computer Engineering at Northwestern University, USA. Dr. Sharma received his Ph.D. degree in 2013 from the Indian Institute of Technology, Delhi, India. He worked as a visiting researcher at Indian Institute of Space science and Technology (IIST) India. His research interests include image processing, image enhancement, phase retrieval, compressive sensing, computational and high resolution imaging.



**Oliver Cossairt** is an Assistant Professor at Northwestern University. Before joining Northwestern, he earned a Masters degree at the MIT Media Lab. He earned his Ph.D. from Columbia University, where he was awarded an NSF Graduate Research Fellowship. Prof. Cossairt is the director of the Computational Photography Laboratory at Northwestern University, and his research interests include optics/photonics, computer graphics, computer vision, and image processing.



**Nathan Matsuda** is a Ph.D. candidate and NSF graduate research fellow at Northwestern University in Prof. Ollie Cossairt's computational photography lab. Nathan's work includes real-time 3D scanning in challenging environments, low-cost surface characterization for cultural heritage applications, and novel 3D displays for virtual reality systems. Prior to grad school, Nathan worked as a visual effects artist with over two dozen credits in film and television, including a primetime Emmy nomination for ABC's Once Upon A Time.



**Ashok Veeraraghavan** is currently an Assistant Professor of Electrical and Computer Engineering at Rice University where he directs the Computational Imaging and Vision Lab. His research interests include computational imaging, computer vision and scaleable health. He received his Bachelors in Electrical Engineering from the Indian Institute of Technology, Madras in 2002 and M.S and Ph.D. degrees from the Department of Electrical and Computer Engineering at the University of Maryland, College Park in 2004 and 2008 respectively.